An Evolved Artificial Radical Cyclase Enables the Construction of Bicyclic Terpenoid Scaffolds via an H-Atom Transfer Pathway

Dongping Chen[‡2,3], Xiang Zhang[‡2,3], Anastassia Andreevna Vorobieva[4,5], Ryo Tachibana[2,3], Alina Stein[3], Roman P. Jakob[7], Zhi Zou[1,3], Damian Alexander Graf[1,3], Ang Li[8], Timm Maier[7], Bruno E. Correia*[6], Thomas R. Ward*[1,2,3]

[1] National Center of Competence in Research "Molecular Systems Engineering", 4058 Basel, Switzerland.

[2] National Center of Competence in Research "Catalysis", Switzerland.

[3] Department of Chemistry, University of Basel, BPR 1096, Mattenstrasse 22, 4002 Basel, Switzerland.

[4] Structural Biology Brussel, Vrije Universiteit Brussel, Brussels, Belgium.

[5] VUB-VIB Center for Structural Biology, Brussels, Belgium.

[6] Institute of Bioengineering, École Polytechnique Fédérale de Lausanne, Lausanne CH-1015, Switzerland.

[7] Biozentrum, University of Basel, Basel, Switzerland.

[8] State Key Laboratory of Chemical Biology, Shanghai Institute of Organic Chemistry, University of Chinese Academy of Sciences, Chinese Academy of Sciences, Shanghai 200032, China

‡ D. C. and X. Z. contributed equally to this paper.

Email: thomas.ward@unibas.ch. bruno.correia@epfl.ch

ABSTRACT: While natural terpenoid cyclases generate complex terpenoid structures via cationic mechanisms, alternative radical cyclization pathways are underexplored. The metal-catalyzed hydrogen-atom-transfer (M-HAT) reaction offers an attractive means for hydrofunctionalizing olefins, providing access to terpenoid-like structures. Artificial metalloenzymes offer a promising strategy for introducing M-HAT reactivity into a protein scaffold. Herein, we report our efforts towards engineering an artificial radical cyclase (ARCase), resulting from anchoring a biotinylated [Co(Schiff-base)] cofactor within an engineered chimeric streptavidin. After two rounds of directed

evolution, a double mutant catalyzed a radical cyclization to afford bicyclic products with a *cis*-5-6-fused ring structure and up to 97% enantiomeric excess. The involvement of a histidine ligation to the Co-cofactor was confirmed by crystallography. A time-course experiment revealed a cascade reaction catalyzed by the ARCase, combining a radical cyclization with a conjugate reduction. The ARCase exhibited tolerance towards variations in the dienone substrate, highlighting its potential to access terpenoid scaffolds.

■ INTRODUCTION

Terpenoids and their derivatives comprise a vast group of over 80,000 members with diverse molecular structures and interesting bioactivities that significantly impact human lives.[1] Among the diverse terpenoid structures, the *cis*-5-6-fused ring scaffold is one of the most represented skeletons, enabling access to structurally diverse terpenes, Figure 1a.[2] In nature, diverse enzymes are used to process terpenes. In particular, terpene cyclases enable the assembly of the core polycyclic scaffold from isoprene units, Figure 1b.[3] The cationic mechanism plays a crucial role in terpenoid cyclase, affording diverse polycyclic structures, including the *cis*-5-6-fused ring.[2,3] To complement the broad repertoire of reactions proceeding via a cationic mechanism, radical-based enzymatic catalysis has gained increasing attention recently.[4-6] Native enzymes have been repurposed to catalyze challenging enantioselective radical reactions initiated by halogen atom abstraction.[7-10] To the best of our knowledge, enzymatic radical reactions resulting from an H-atom transfer on an unactivated olefin to access terpenoid scaffolds have not been reported to date.

The metal-hydride hydrogen-atom-transfer triggered radical reaction (M-HAT) is a powerful strategy for the hydrofunctionalization of olefins.[11-16] In this process, a metal-hydride initially transfers a hydrogen atom to an unactivated olefin with Markovnikov selectivity.[17] The resulting carbon-centered radical can react with various radical acceptors, thus offering an attractive means to convert olefins into diverse functional groups, Figure 1c.[18,19] However, stereoselective control over the functionalization of the carbon-centered radical intermediate is challenging.[20-23] Compared to homogenous catalysis, enzymes provide opportunities for precise stereocontrol via secondary sphere interactions[24] between the protein and the fleeting radical species. Pioneered by Wilson and Whitesides,[25] artificial metalloenzymes (ArMs) offer attractive means to combine features of both homogeneous and enzyme catalysts. ArMs result from incorporating an abiotic metal cofactor into a macromolecular scaffold.[26-32] In this context, ArMs based on the biotin-streptavidin technology have been designed and evolved to catalyze a broad range of abiotic reactions.[33] Herein, we report on an Artificial Radical Cyclase (ARCase) that results from the incorporation of a biotinylated [Co(Schiff-base)] cofactor into an engineered streptavidin host (Figure 1d).

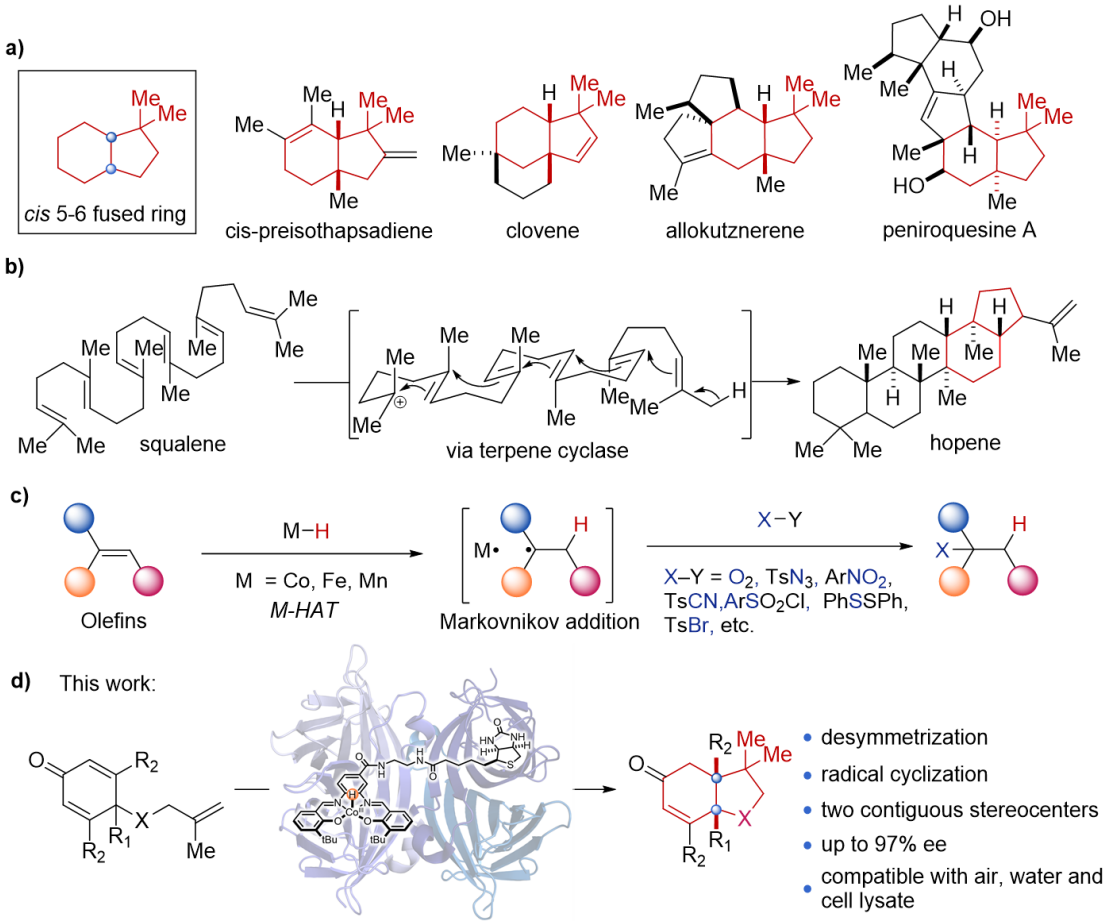

Figure 1. An artificial radical cyclase designed for the asymmetric construction of terpenoid architectures. a) Selected terpenoid natural products containing a *cis*-5-6 fused ring scaffold. b) Representative biosynthetic pathway of terpene proceeding via a cationic cyclization. c) Illustrative Metal-catalyzed Hydrogen-Atom Transfer reaction-based radical reactions (M-HAT). d) An artificial radical cyclase-promoted assembly of an enantiopure terpenoid structure with a *cis*-5-6 fused ring.

■ RESULTS AND DISCUSSION

Design of the ARCase. Various desymmetrization strategies have been exploited to generate enantioenriched structures from prochiral starting materials in organic synthesis.[34] The dienone scaffold, an outstanding Michael acceptor for nucleophiles, has also proved to be an excellent radical acceptor.[15] Capitalizing on the symmetry of the dienone group, we envisioned that substrate **1** may undergo a Markovnikov HAT on the terminal alkene, followed by an intramolecular Giese addition[35] to afford the corresponding *cis*-5-6-fused bicyclic product **2**, Figure 1d. Notably, the cyclization product **2** was reported as a key intermediate in the synthesis of the terpenoid natural product $\Delta^{9(12)}$-capnellane.[36] With this goal in mind, we synthesized five biotinylated [Co(Schiff-base)] cofactors **3-7** for an initial evaluation.[11,20-22] The screening was conducted using [Co(Biotin-Schiff-base)] cofactors **3-7** under aqueous and aerobic

Table 1. Initial chemogenetic optimization of ARCase activity.[a]

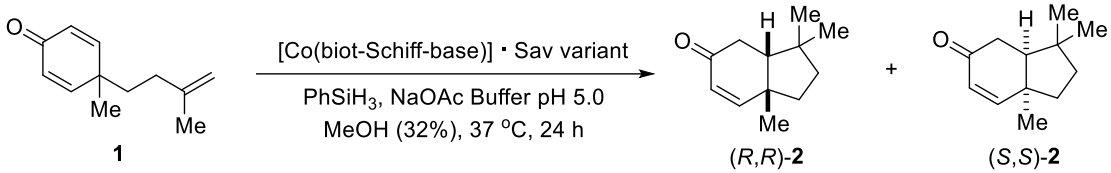

Entry	[Co(Biot-Schiff-base)] · Sav variant	Yield (%)	e.r. (*R*,*R*)/(*S*,*S*)
1	[Co(Biot-en-^{t}Bu$_4$-Salphen)] **3**	3	-
2	[Co(Biot-en-^{t}Bu$_2$-Salphen)] **4**	8	-
3	[Co(Biot-en-Me-Salphen)] **5**	0	-
4	[Co(Biot-NN-^{t}Bu$_2$-Salphen)] **6**	5	-
5	[Co(Biot^{C5}-^{t}Bu$_2$-Salphen)] **7**	3	-
6	[Co(Biot-en-^{t}Bu$_4$-Salphen)] **3** · Sav WT	19	50:50
7	[Co(Biot-en-^{t}Bu$_2$-Salphen)] **4** · Sav WT	12	48:52
8	[Co(Biot-en-Me-Salphen)] **5** · Sav WT	0	-
9	[Co(Biot-NN-^{t}Bu$_2$-Salphen)] **6** · Sav WT	9	51:49
10	[Co(Biot^{C5}-^{t}Bu$_2$-Salphen)] **7** · Sav WT	10	48:52
11	[Co(Biot-en-^{t}Bu$_2$-Salphen)] **4** · Sav K121H	51	54:46
12	[Co(Biot-en-^{t}Bu$_2$-Salphen)] **4** · Sav K121F	28	47:53
13	[Co(Biot-en-^{t}Bu$_4$-Salphen)] **3** · Sav K121H	30	48:52
14[b]	[Co(Biot-en-^{t}Bu$_2$-Salphen)] **4** · Sav K121H	46	72:28
15[b]	[Co(Biot-en-^{t}Bu$_2$-Salphen)] **4** · Sav S112H	17	32:68

[a]Unless otherwise stated, the standard reaction conditions were: Sav WT (20 μM), [Co(Biot-en-^{t}Bu$_2$-Salphen)] **4** (5 μM, 0.5 mol %), substrate **1** (1 mM), PhSiH$_3$ (80 mM), NaOAc buffer (pH 5.0)/MeOH (274 μL/120 μL), 37 °C for 24 h. [b]The reaction was performed with 1 mol % catalyst loading at 10 °C. All the experiments were performed in duplicate.

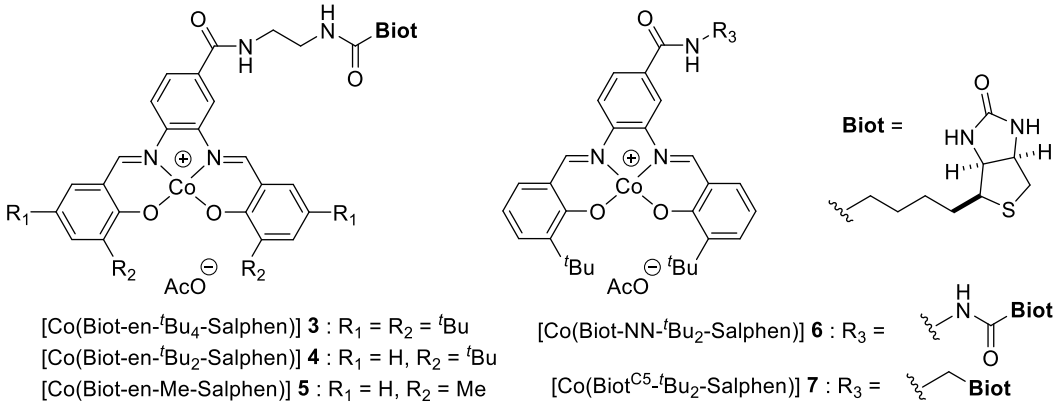

conditions (entries 1-5, Table 1). Four cofactors afforded the desired cyclization product **2**, albeit in low yield. Gratifyingly, upon incorporation in streptavidin wild-type (Sav WT hereafter), the yield was improved for all cofactors except **5** (Table 1, entries 6-10), highlighting the positive impact of the hydrophobic environment provided by Sav. However, no significant enantioselectivity was observed. Steric considerations led us to select [Co(Biot-en-^{t}Bu$_2$-Salphen)] **4** over cofactor **3** for subsequent protein engineering efforts, despite its slightly reduced activity. Importantly, upon incorporation of [Co(Biot-en-^{t}Bu$_2$-Salphen)] **4** with Sav WT, the stability of cofactor was positively affected, minimizing its decomposition in aqueous medium (Supplementary Figure S3). Next, residues at positions Sav S112 and K121 were selected for the initial genetic optimization of ARCase.[33] The single variant [Co(Biot-en-^{t}Bu$_2$-Salphen)] **4** · Sav K121H afforded the bicyclic product **2** in 51% yield, albeit with low enantioselectivity (Table 1, entry 11). To evaluate the possibility of a π–π interaction between the cofactor and K121H, we tested [Co(Biot-en-^{t}Bu$_2$-Salphen)] **4** · Sav K121F, which proved significantly less active than the Sav K121H-based ARCase (Table 1, entry 12). This led us to hypothesize that the histidine residue Sav K121H may coordinate with the cobalt. Next, the influence of various reaction parameters was investigated to improve ARCase activity in the presence of [Co(Biot-en-^{t}Bu$_2$-Salphen)] **4** · Sav K121H (Supplementary Table S8-11). Gratifyingly, the e.r. increased to 72:28 upon decreasing the temperature to 10 °C (Table 1, entry 14). The absolute configuration of the major enantiomer was determined as (*R*, *R*)-**2** by vibrational circular dichroism (Supplementary Figure S8). Interestingly, [Co(Biot-en-^{t}Bu$_2$-Salphen)] **4** · Sav S112H afforded the opposite enantiomer (*S*, *S*)-**2** (Table 1, entry 15) .[33]

Engineering a chimeric loop to shield the active site of the ARCase. The positive influence of the protein on ARCase performance led to further optimization through structural engineering of Sav. To shield the biotin-binding vestibule where the cofactor is located, we sought to engineer a chimeric loop surrounding the cofactor using computational protein design.[37-40] We developed a pipeline in Rosetta to insert and optimize loops and small domains of variable length between two cut points in a protein. The Direct Segment Lookup application was used to search an internal database for fragments geometrically-matching the defined cut points and generate stable and rigid fusions (Figure 2a). The loop involved in biotin-binding (i.e. loop ¾) was selected as the insertion site because of its tolerance to structure variability observed across the avidin family. The search resulted in 1700 grafts with high secondary structure content and no clashes with the scaffold. The inserted fragments, which were taken out of their native protein context, were further optimized in the context of the C_2-streptavidin dimer by iterative local conformational sampling and combinatorial sequence design.

One hundred thirty-five unique grafts make favorable contacts to the scaffold, and the symmetric partners were selected for experimental characterization. The inserted fragments introduced additional 9 to 16 C_β contacts to cobalt within 10 Å (Figure 2b-2c) and were 5 to 30 residue-long (Figure 2d-2e). Thirty-two short loops (< 10 residues) and 103 larger grafts (10-30 residues) were ordered as synthetic genes and expressed in *E. coli*. Most of the short (75%) and long (86%) inserts were expressed and showed conserved biotin-binding activity in *E. coli* lysate using biotin-4-fluorescein (B4F). By contrast, previous attempts to insert fragments in the same Sav loop using flexible linkers resulted in 75% and 40% soluble-expressed and functional short and long loop chimeras, respectively.[38] Hence, our computational pipeline consisting of geometric matching of the fragments to cut sites to design rigid and optimized linkers enables the grafting of structurally diverse large fragments with an increased success rate.

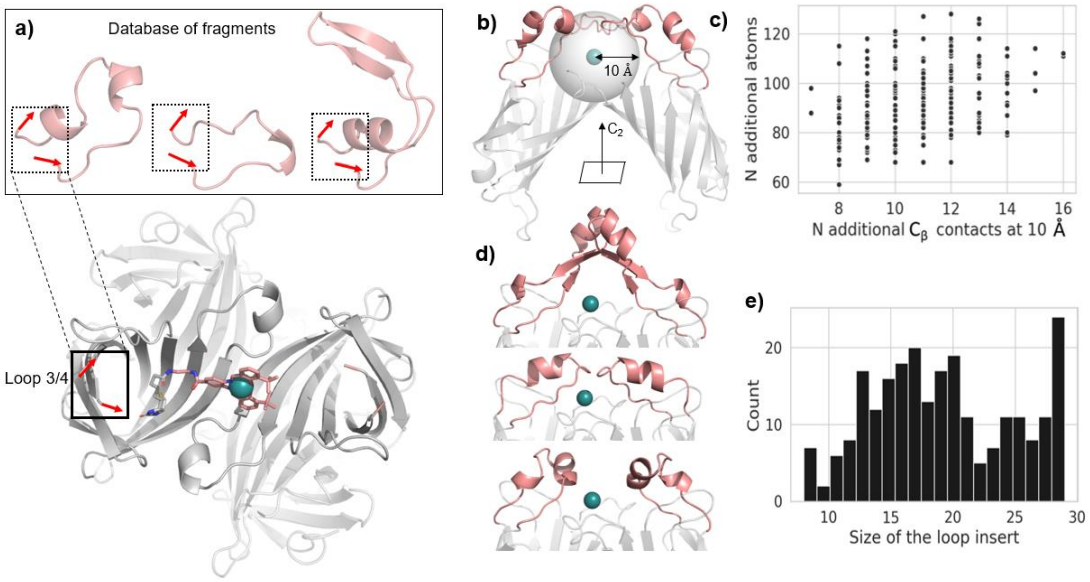

Figure 2. Engineering a chimeric loop to shield the active site of the ARCase. a) Computational grafting pipeline. Selected cut points in loop ¾ (red arrows) are geometrically matched to a database of fragments. The biotinylated cofactor bound to Sav is shown as sticks (grey: buried biotin; salmon: solvent-exposed cofactor). The Co atom is displayed as a teal sphere. b-c) Number of new C_β and atom contacts within 10 Å of the Co atom in the chimeric Sav library, in the context of the C_2 symmetry of one catalytic unit. d) Examples of grafted loops with C_2 symmetry. e) Distribution of inserts lengths in the library.

Genetic Optimization of the ARCase. Capitalizing on the significant improvement of ARCase activity in the presence of the Sav K121H mutation (Sav* hereafter), a histidine residue at this position was introduced in the *in silico*-designed chimeric Sav library (chSav hereafter, chSav* including the histidine mutation). The ARCase

performance of chSav* for the radical cyclization of dienone **2** was evaluated in the presence of [Co(Biot-en-^{t}Bu$_2$-Salphen)] **4**. To streamline the workflow, we tested whether *E. coli* cell-free extracts (CFE) could be used to screen and rapidly identify promising chSav* (Supplementary Table S12). Relying on a 24 well-plate protocol, chSav* which yielded ≥ 20 µM free biotin-binding sites were evaluated in the presence of [Co(Biot-en-^{t}Bu$_2$-Salphen)] **4**, Figure 3a. As can be appreciated, certain chSav* outperformed Sav*, both in terms of activity and/or selectivity, Figure 3b. The most promising variants (chSav*1, chSav*2 and chSav*3) were expressed and purified to validate the CFE screening. We selected chSav*2 for further protein engineering efforts. As this chimera is endowed with a mostly α-helical sixteen amino acid insert to replace the original residues from 48 to 53, it is abbreviated chSav*_α_{16} (Supplementary Figure S1). This insert affects the amino acid numbering of the Sav: positions S112 and K121H are labeled S122 and K131H for chSav_α_{16}, respectively (Supplementary Figure S1). Next, the genetic optimization of ARCase's performance relying either on Sav or chSav_α_{16} was carried out, Figure 3c. In the presence of [Co(Biot-en-^{t}Bu$_2$-Salphen)] **4**, chSav_α_{16} WT (K131) exhibited higher TON than Sav WT, albeit with lower e.e. Introduction of a potentially coordinating-histidine residue led to a pronounced improvement in the e.e. with [Co(Biot-en-^{t}Bu$_2$-Salphen)] **4** · chSav*_α_{16} K131H (from –4% to 74% e.e.), contrasting with a modest improvement with Sav* K121H (from 22% to 44% e.e.). For the second round of mutagenesis, we randomized position S122 in chSav*_α_{16} S122X-K131H and the corresponding S112 in Sav* S112X-K121H. To our delight, the cyclization product (*R, R*)-**2** was obtained in 97% e.e. in the presence of [Co(Biot-en-^{t}Bu$_2$-Salphen)] **4** · chSav*_α_{16} S122V-K131H, compared to 81% e.e. for the non-chimeric Sav* S112V-K121H.

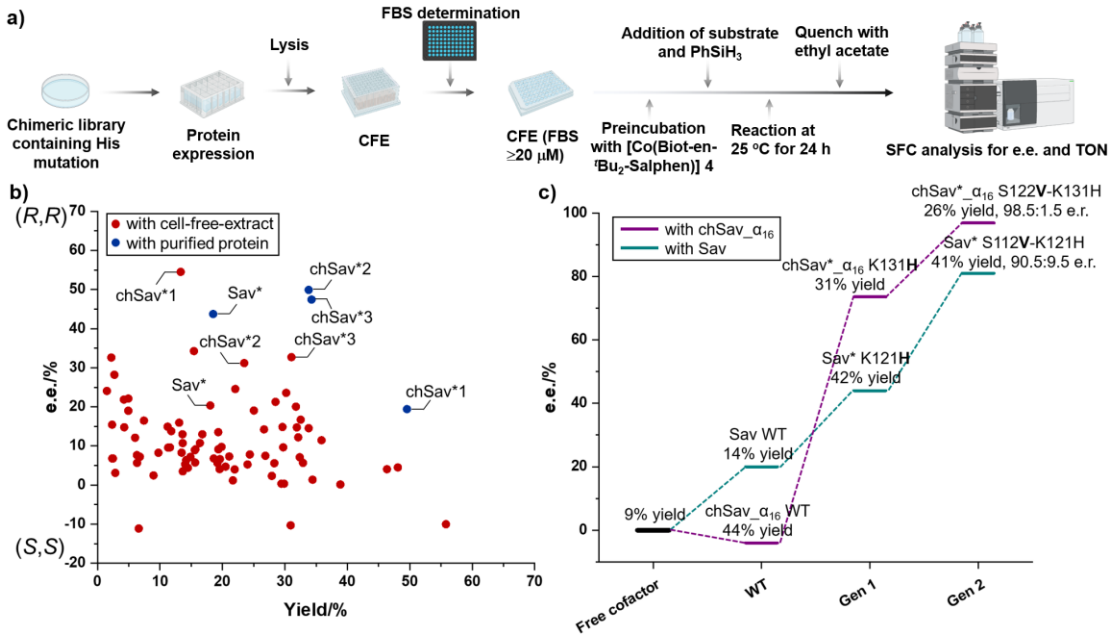

Figure 3. Genetic optimization of ARCase performance by protein engineering using

[Co(bio-en-^{t}Bu$_2$-salphen)] **4** as cofactor. a) A 24-well plate screening workflow enables the expression and evaluation of the ARCase performance using cell-free extracts (CFE). Following expression, the biotin-binding capacity (FBS) was determined by fluorescence using biotin-4-fluorescein. Samples with ≥ 20 μM FBS were selected for screening. b) Scatterplot of ARCase activity and enantioselectivity at 25 °C using various chimeric Sav bearing a histidine mutation (chSav*) in CFE (red) and selected purified variants (blue). c) Comparison of the evolutionary trajectory for the ARCase performance for [Co(Biot-en-^{t}Bu$_2$-Salphen)] **4** · chSav_α_{16} (purple) and [Co(Biot-en-^{t}Bu$_2$-Salphen)] **4** · Sav (green) at 10 ºC.

Structural analysis of the evolved ARCase [Co(Biot-en-^{t}Bu$_2$-Salphen)] 4 · chSav*_α_{16} S122V-K131H. To scrutinize the influence of the Sav host protein on the anchored cofactor, a QM/MM calculation was performed on [Co(Biot-en-^{t}Bu$_2$-Salphen)] **4** · chSav*_α_{16} S122V-K131H, Figure 4a (See Supplementary Information section 6 for details). Gratifyingly, the calculation confirmed the axial coordination of the engineered histidine residue K131H to the cobalt ion. The first coordination sphere is thus reminiscent of the naturally-occurring cobalamin cofactor.[41] The inserted loop α_{16} (highlighted in salmon) partially shields the cofactor, potentially influencing the catalytic performance, Figure 3c. To validate the QM/MM studies, the evolved ARCase was crystallized by soaking [Co(Biot-en-^{t}Bu$_2$-Salphen)] **4** in crystals of the apo chSav*_α_{16} S122V-K131H (Supplementary Table S1). Gratifyingly, the resulting single X-ray crystal structure (1.9 Å resolution, PDB 8QEX) confirmed the axial coordination of histidine K131H of monomer A (K131H^A) to the cobalt ion bound to the monomer A of chSav*, Figure 4b. The RMSD between the calculated structure and the X-ray structure was computed at 1.36 Å. The X-ray structure reveals a single cofactor **4** bound to monomer Sav^A and K131H^A, and localized within the biotin-binding vestibule consisting of both monomers Sav^A and Sav^B: the cofactor is positioned near the interface of the two monomers. Additional short contacts between the cofactor **4** and the host protein include: chSav S122V, K131H^B, L120, S132, T133, L134, Figure 4c. These close contacts possibly contribute to the firm localization of the [Co(Biot-en-^{t}Bu$_2$-Salphen)] **4** within the chSav* scaffold. Unfortunately, the chimeric loop could not be fully resolved in the X-ray structure due to its high flexibility. Although the orientation of cofactor **4** exhibits some variation between the QM/MM and X-ray structures, we surmise that the inserted loop α_{16} indeed can shield the active site during the enantiodetermining step, Figure 4d.

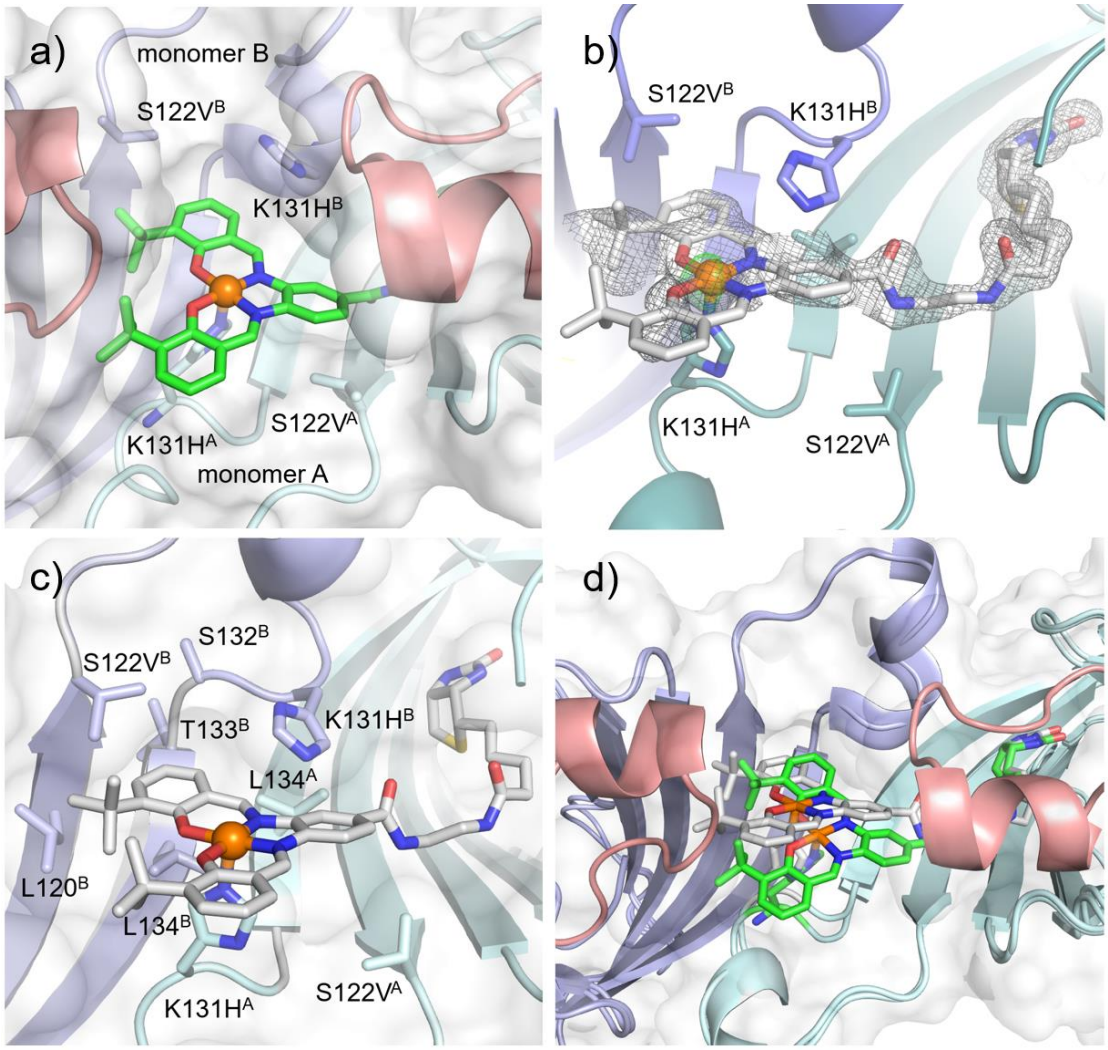

Figure 4. Structural analysis of the evolved ARCase. a) QM/MM calculation of the model structure of dimer chSav*_α_{16} S122V-K131H with a single [Co(Biot-en-^{t}Bu$_2$-Salphen)] **4** bound. b) X-ray crystal structure of chSav*_α_{16} S122V-K131H and [Co(Biot-en-^{t}Bu$_2$-Salphen)] **4**. c) Close-up view of the X-ray structure highlighting the close contacts between [Co(Biot-en-^{t}Bu$_2$-Salphen)] **4** and chSav*_α_{16} S122V-K131H. d) Overlay of the QM/MM calculated structure and X-ray structure. The protein is displayed as cartoon and transparent surface. Monomer B is displayed in light-blue and monomer A in cyan. The α_{16} loop is displayed in salmon for the QM/MM structure, and is disordered in the X-ray structure. [Co(Biot-en-^{t}Bu$_2$-Salphen)] **4** is represented as green sticks for the computed structure and as grey sticks in the X-ray structure (atoms are color-coded: nitrogen = blue, oxygen = red, sulfur = yellow, cobalt = orange). The 2Fo−Fc electron-density map is displayed as a black mesh (1σ), and the anomalous electron density is displayed as a green mesh (3σ) assigned to cobalt. The occupancy of the cobalt was set to 50%.

Time-course monitoring of ARCase activity. We were intrigued that, throughout the

evolutionary trajectory, the improvement in enantioselectivity was accompanied with an erosion in TON, Figure 3c. This prompted further investigation into the mechanistic details of the radical cyclization. Monitoring of reaction progress by chiral GC-FID rather than HPLC revealed that the conjugate reduction product **8** (Figure 5a) was formed in varying amounts, depending on the nature of the host protein. Independent experiments using the enone cyclization product **2** as the substrate and ARCase revealed the formation of the reduction product **8** (Supplementary Scheme S7). Such M-HAT-based conjugate reduction reactions have been reported with homogenous catalysts.[16] To investigate the possibility of a concurrent dual M-HAT mechanism, we monitored the product distribution in the presence of [Co(Biot-en-^{t}Bu$_2$-Salphen)] **4** · chSav*_α_{16} S122V-K131H over time, Figure 5b. The dienone **1** was consumed within 20 minutes and was completely depleted within an hour. The maximum yield of the bicyclic enone **2** was reached after 30 minutes. After that, the conjugate addition product **8** was formed, resulting in an erosion in the yield of enone **2**. Gratifyingly, the second M-HAT leading to the ketone **8** proceeds stereoselectively, leading to the preferential consumption of the minor diastereomer (*S*, *S*)-**2**, Figure 5a. The selectivity factor for the kinetic resolution was s = 4, Figure 5b (Supplementary Table S15).[42]

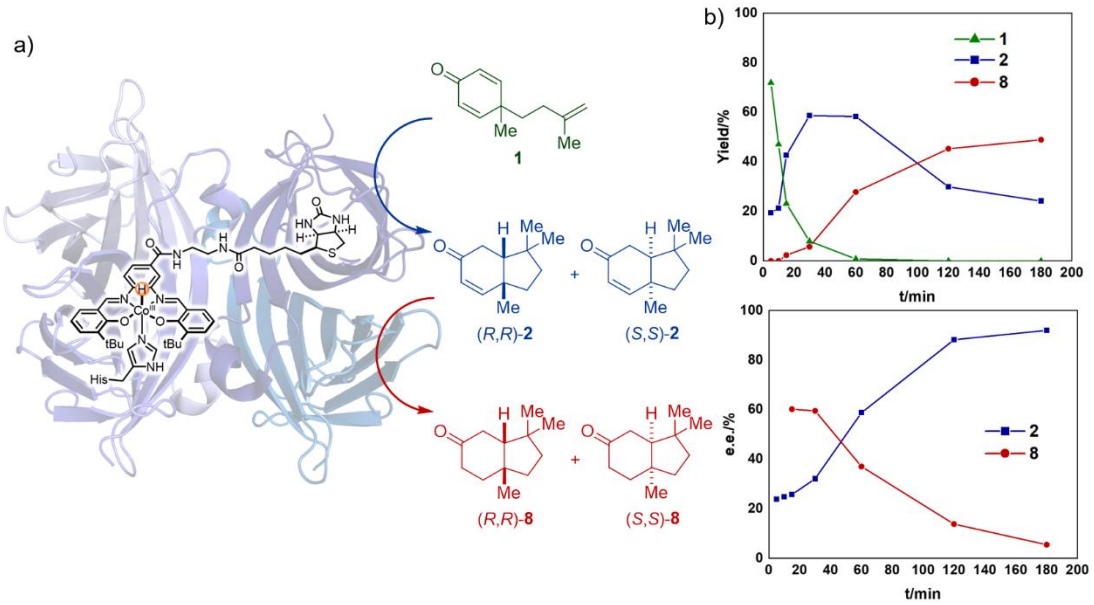

Figure 5. Asymmetric radical cyclization of dienone **1** and kinetic resolution of the cyclized enone **2** to the corresponding ketone **8**. a) [Co(Biot-en-^{t}Bu$_2$-salphen)] **4** · chSav*_α_{16} S122V-K131H catalyzed cascade reaction consisting of a radical cyclization followed by a conjugate reduction. b) Time-course monitoring of ARCase progress, product-distribution (top) and enantioselectivity (bottom).

Substrate scope. To further explore the performance of the engineered ARCase, several prochiral substrates that afford bicyclic products **9**-**14** with a *cis*-5-6 fused ring

structure were examined, Figure 6a. These featured diverse side chains, an ether moiety that links the dienone to the terminal olefin, and substituents on the dienone moiety. The substrate containing an extended methylether side-chain, afforded the cyclization product **9** in very good e.r. (93:7 e.r.) and 46% yield. Substituting the methoxyl with an acetyl group, product **10** was obtained in a comparable yield and selectivity (39% and 90:10 e.r., respectively). The enone **11** with a slightly shorter side-chain was produced in higher yield (58%) but significantly lower e.r. (67:33 e.r.). The ether-substituted side chain also proved compatible with the ARCase. The enone **12** was produced with a good e.r. and yield (88:12 e.r. and 46%, respectively). Taking advantage of an ether linkage, the tetrahydrofuran **13** was obtained in moderate selectivity (81:19 e.r.), albeit in low yield (17%). Introducing a methyl group on both sides of the prochiral dienone moiety afforded furan **14**, containing two contiguous quaternary centers, in 44% yield, albeit as a racemate. For the latter two substrates, [Co(Biot-en-^{t}Bu$_2$-salphen)] **4** · chSav*_α_{16} S122A-K131H outperformed the chSav*_α_{16} S122V-K131H ARCase variants used otherwise.

A scale up reaction was performed with the ARCase [Co(Biot-en-^{t}Bu$_2$-salphen)] **4** · chSav*_α_{16} S122V-K131H and substrate **15**, Figure 6b. The bicyclic product **9** was isolated in 48% yield and 90:10 e.r. Subsequent deprotection of the methoxy group with BBr_3, provided the tricyclic compound **16** in 74% yield and good selectivity (92:8 e.r.). Notably, this congested tricyclic ring scaffold has been identified in several natural products,[43,44] including the terpenoid cumbiasin C.[43] Hence, the ARCase-based chemo-enzymatic strategy offers a promising avenue for the asymmetric construction of polycyclic structures, potentially expediting the synthesis of natural products and medicinal compounds.

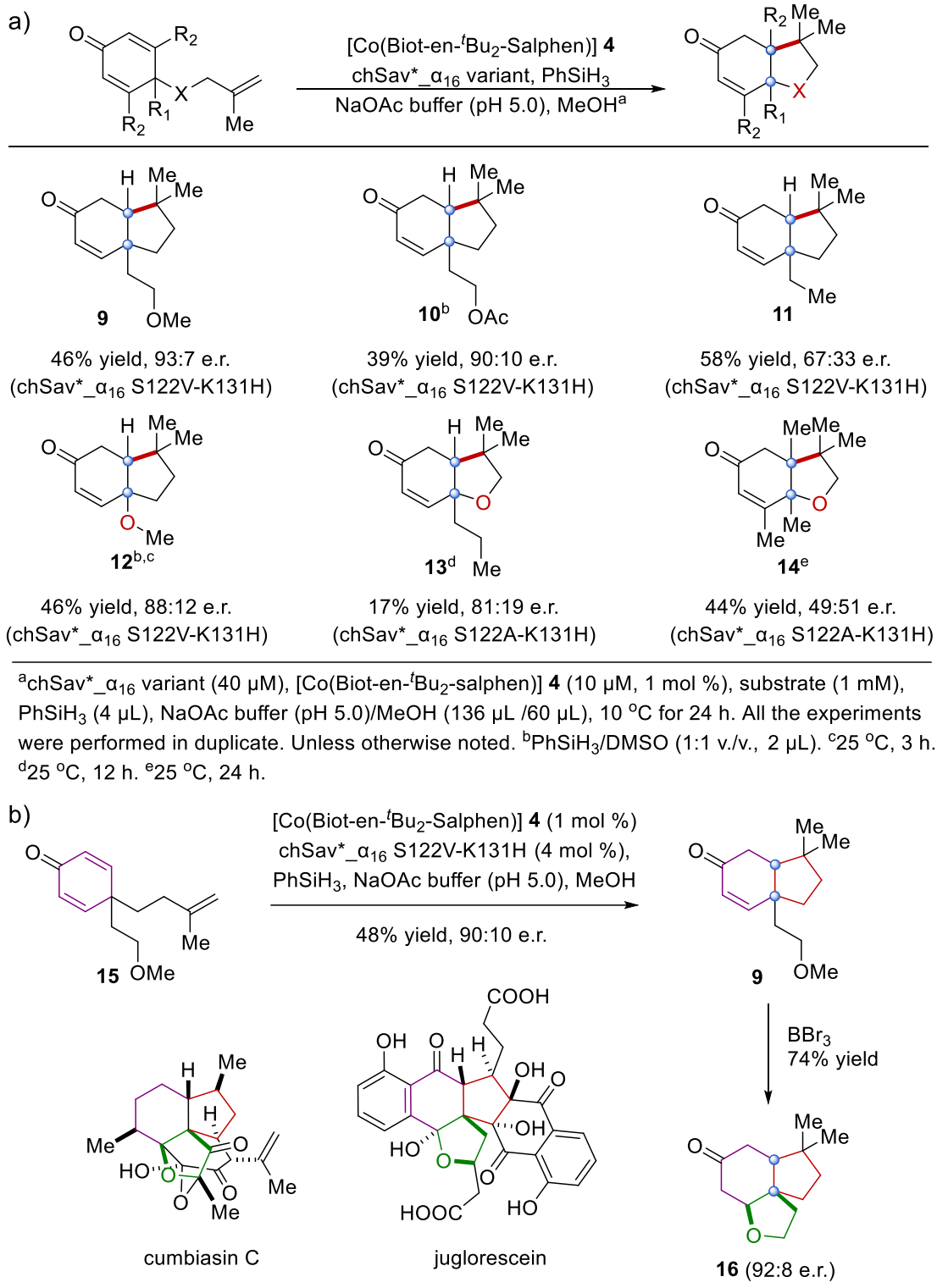

Figure 6. Application of ARCases towards construction of terpenoid-like structures. a) Substrate scope with selected ARCases. b) A chemo-enzymatic approach for the assembly of an enantiopure tricyclic ring scaffold via ARCase.

■CONCLUSION

Relying on alkenes as radical initiators, M-HAT-based radical reactions have proven

versatile for accessing polycyclic structures.[45] However, mastering enantioselective radical cyclizations using homogeneous catalysis remains challenging.[46,47] In a biomimetic spirit, the artificial radical cyclase presented herein combines the reactivity of an abiotic Co–H cofactor, with a well-defined second coordination sphere provided an evolved protein scaffold. The axial histidine ligation to Co(III) proved essential in improving the performance of the ARCase, by firmly anchoring the abiotic cofactor within a chimeric streptavidin endowed with a hydrophobic lid covering the active site. The Co-cofactor, and its histidine-coordination, bears striking resemblance to cobalamin, both in terms of first coordination sphere and in catalytic prowess, providing access to stereoselective radical C–C bond-forming reactions.[41] Importantly, the substrate scope and chemo-enzymatic strategy of the evolved ARCase open promising perspectives towards synthesizing diverse enantiopure terpenoid building blocks.

■DATA AVAILABILITY

The data that support the findings in this study are available within this article and the Supplementary Information. Crystallographic data for the ARCase structure of [Co(Biot-en-^{t}Bu$_2$-Salphen)] **4** · chSav*_α_{16} S122V-K131H reported in this article have been deposited at the Protein Data Bank under the code: 8QEX.

■REFERENCE

1 Breitmaier, E. *Terpenes: flavors, fragrances, pharmaca, pheromones*. 1-223 (Wiley-VCH, 2006).

2 Le Bideau, F., Kousara, M., Chen, L., Wei, L. & Dumas, F. Tricyclic sesquiterpenes from marine origin. *Chem. Rev.* **117**, 6110-6159 (2017).

3 Christianson, D. W. Structural and chemical biology of terpenoid cyclases. *Chem. Rev.* **117**, 11570-11648 (2017).

4 Chen, K. & Arnold, F. H. Engineering new catalytic activities in enzymes. *Nat. Catal* **3**, 203-213 (2020).

5 Emmanuel, M. A. et al. Photobiocatalytic strategies for organic synthesis. *Chem. Rev.* **123**, 5459-5520 (2023).

6 Zetzsche, L. E. et al. Biocatalytic oxidative cross-coupling reactions for biaryl bond formation. *Nature* **603**, 79-85 (2022).

7 Ye, Y. X. et al. Using enzymes to tame nitrogen-centred radicals for enantioselective hydroamination. *Nat. Chem* **15**, 206-212 (2023).

8 Zhou, Q., Chin, M., Fu, Y., Liu, P. & Yang, Y. Stereodivergent atom-transfer radical cyclization by engineered cytochromes P450. *Science* **374**, 1612-1616 (2021).

9 Rui, J. Y. et al. Directed evolution of nonheme iron enzymes to access abiological radical-relay C(sp^3)-H azidation. *Science* **376**, 869-874 (2022).

10 Huang, X. Q. et al. Photoenzymatic enantioselective intermolecular radical hydroalkylation. *Nature* **584**, 69-74 (2020).

11 Crossley, S. W. M., Obradors, C., Martinez, R. M. & Shenvi, R. A. Mn-, Fe-, and Co-catalyzed radical hydrofunctionalizations of olefins. *Chem. Rev.* **116**, 8912-9000 (2016).

12 Mukaiyama, T. et al. Oxidation-reduction hydration of olefins with molecular-oxygen and 2-propanol catalyzed by bis(acetylacetonato)cobalt(II). *Chem. Lett.* **18**, 449-452 (1989).

13 Waser, J. & Carreira, E. M. Convenient synthesis of alkylhydrazides by the cobalt-catalyzed hydrohydrazination reaction of olefins and azodicarboxylates. *J. Am. Chem. Soc.* **126**, 5676-5677 (2004).

14 Ishikawa, H. et al. Total synthesis of Vinblastine, Vincristine, related natural products, and key structural analogues. *J. Am. Chem. Soc.* **131**, 4904-4916 (2009).

15 Lo, J. C., Yabe, Y. & Baran, P. S. A practical and catalytic reductive olefin coupling. *J. Am. Chem. Soc.* **136**, 1304-1307 (2014).

16 Ma, X. S. & Herzon, S. B. Intermolecular hydropyridylation of unactivated alkenes. *J. Am. Chem. Soc.* **138**, 8718-8721 (2016).

17 Choi, J. W., Tang, L. H., Norton, J. R. . Kinetics of hydrogen atom transfer from (η^5-C_5H_5)$Cr(CO)_3H$ to various olefins: influence of olefin structure. *J. Am. Chem. Soc.* **129**, 234-240 (2007).

18 Kim, D., Rahaman, S. M. W., Mercado, B. Q., Poli, R. & Holland, P. L. Roles of Iron complexes in catalytic radical alkene cross-coupling: a computational and mechanistic study. *J. Am. Chem. Soc.* **141**, 7473-7485 (2019).

19 Shevick, S. L. et al. Catalytic hydrogen atom transfer to alkenes: a roadmap for

metal hydrides and radicals. *Chem. Sci* **11**, 12401-12422 (2020).

20 Discolo, C. A., Touney, E. E. & Pronin, S. V. Catalytic asymmetric radical-polar crossover hydroalkoxylation. *J. Am. Chem. Soc.* **141**, 17527-17532 (2019).

21 Ebisawa, K. et al. Catalyst- and silane-controlled enantioselective hydrofunctionalization of alkenes by cobalt-catalyzed hydrogen atom transfer and radical-polar crossover. *J. Am. Chem. Soc.* **142**, 13481-13490 (2020).

22 Qin, T. et al. Cobalt-catalyzed radical hydroamination of alkenes with *N*-fluorobenzenesulfonimides. *Angew. Chem. Int. Ed.* **60**, 25949-25957 (2021).

23 Mondal, S., Dumur, F., Gigmes, D., Sibi, M. P., Bertrand, M. P. & Nechab, M. . Enantioselective radical reactions using chiral catalysts. *Chem. Rev.* **122**, 5842–5976 (2022).

24 Stappen, C. V. et al. Designing artificial metalloenzymes by tuning of the environment beyond the primary coordination sphere. *Chem. Rev.* **122**, 11974–12045 (2022).

25 Wilson, M. E. & Whitesides, G. M. Conversion of a protein to a homogeneous asymmetric hydrogenation catalyst by site-specific modification with a diphosphinerhodium(I) moiety. *J. Am. Chem. Soc.* **100**, 306-307 (1978).

26 Schwizer, F. et al. Artificial metalloenzymes: reaction scope and optimization strategies. *Chem. Rev.* **118**, 142-231 (2018).

27 Studer, S. et al. Evolution of a highly active and enantiospecific metalloenzyme from short peptides. *Science* **362**, 1285-1288 (2018).

28 Natoli, S. N. & Hartwig, J. F. Noble-metal substitution in hemoproteins: an emerging strategy for abiological catalysis. *Acc. Chem. Res.* **52**, 326-335 (2019).

29 Mirts, E. N., Petrik, I. D., Hosseinzadeh, P., Nilges, M. J. & Lu, Y. A designed heme-[4Fe-4S] metalloenzyme catalyzes sulfite reduction like the native enzyme. *Science* **361**, 1098-1101 (2018).

30 Oohora, K., Onoda, A. & Hayashi, T. Hemoproteins reconstituted with artificial metal complexes as biohybrid catalysts. *Acc. Chem. Res.* **52**, 945-954 (2019).

31 Song, W. J. & Tezcan, F. A. A designed supramolecular protein assembly with in vivo enzymatic activity. *Science* **346**, 1525-1528 (2014).

32 Roelfes, G. LmrR: a privileged scaffold for artificial metalloenzymes. *Acc. Chem. Res.* **52**, 545-556 (2019).

33 Heinisch, T. & Ward, T. R. Artificial metalloenzymes based on the biotin-streptavidin technology: challenges and opportunities. *Acc. Chem. Res.* **49**, 1711-1721 (2016).

34 Shu, T. & Cossy, J. Asymmetric desymmetrization of alkene-, alkyne- and allene-tethered cyclohexadienones using transition metal catalysis. *Chem. Soc. Rev.* **50**, 658-666 (2021).

35 Giese, B. Formation of CC bonds by addition of free radicals to alkenes. *Angew. Chem., Int. Ed. Engl.* **22**, 753-764 (1983).

36 Salahi, F., Yao, C., Norton, J. R. & Snyder, S. A. The synthesis of diverse terpene architectures from phenols. *Nat. Synth* **1**, 313-321 (2022).

37 Christoffel, F. et al. Design and evolution of chimeric streptavidin for protein-enabled dual gold catalysis. *Nat. Catal* **4**, 643-653 (2021).

38 Pellizzoni, M. M. et al. Chimeric streptavidins as host proteins for artificial metalloenzymes. *ACS Catal.* **8**, 1476-1484 (2018).

39 Grimm, A. R. et al. Cavity size engineering of a β-barrel protein generates efficient biohybrid catalysts for olefin metathesis. *ACS Catal.* **8**, 3358-3364 (2018).

40 Eiben, C. B. et al. Increased diels-alderase activity through backbone remodeling guided by Foldit players. *Nat. Biotechnol* **30**, 190-192 (2012).

41 Demarteau, J., Debuigne, A. & Detrembleur, C. Organocobalt complexes as sources of carbon-centered radicals for organic and polymer chemistries. *Chem. Rev.* **119**, 6906-6955 (2019).

42 Keith, J. M., Larrow, J. F. & Jacobsen, E. N. Practical considerations in kinetic resolution reactions. *Adv. Synth. Catal.* **343**, 5-26 (2001).

43 Rodriguez, A. D., Ramirez, C. & Shi, Y. P. The cumbiasins, structurally novel diterpenes possessing intricate carbocyclic skeletons from the West Indian sea whip Pseudopterogorgia elisabethae (Bayer). *J. Org. Chem.* **65**, 6682-6687 (2000).

44 Kamo, S. et al. Synthetic and biological studies of Juglorubin and related Naphthoquinones. *J. Org. Chem.* **84**, 13957-13966 (2019).

45 Lu, Z. et al. Total synthesis of Aplysiasecosterol A. *J. Am. Chem. Soc.* **140**, 9211-9218 (2018).

46 Lu, H. J. & Zhang, X. P. Catalytic C-H functionalization by metalloporphyrins: recent developments and future directions. *Chem. Soc. Rev.* **40**, 1899-1909 (2011).

47 Lang, K., Hu. Y., Chen Cindy Lee. W., & Zhang. X. P. Combined radical and ionic approach for the enantioselective synthesis of β-functionalized amines from alcohols. *Nat. Synth* **1**, 548-557 (2022).

Acknowledgement

T. R. W. thanks the NCCR Catalysis (Grant Number 180544), a National Centre of Competence in Research funded by the Swiss National Science Foundation. Additional funding was provided by the NCCR Molecular Systems Engineering (Grant Number 200021_178760). X. Z. thanks the SIOC postdoc fellowship for the financial support. R.T. thanks the Naito Foundation for financial support. We acknowledge the Paul Scherrer Institut, Villigen, Switzerland, for provision of synchrotron radiation beamtime at beamline X06SA of the SLS.

Author contributions

T. R. W., X. Z. and D. C. conceived and designed the study. X. Z. contributed to the synthesis of the substrates, products and complexes. D. C. contributed to the mutagenesis and protein expression and protein purification and protein mass. D. C. and X. Z. performed the catalytic, and time course experiment, designed the screening workflow and record the data. T. R. W., X. Z. and D. C. analyzed the data. R. P. J., T.M., and D. C. contributed to the crystallization and crystallographic structural analysis. A. V., B. C., A. S. and T. R. W. contributed to the collaboration on the computational design of chimeric streptavidin. R. T. contributed to the molecular modelling and QM/MM calculation. Z. Z. offered the molecular biology instructions. D. A. G. offered synthetic suggestions. A. L. provided helpful discussion regarding the M-HAT reaction. A. S. established the Chim_Sav library workflow and associated molecular biology methods. T. R. W., X. Z. and D. C. wrote the manuscript, which was further supplemented through contributions from R. P. J., R. T. and A. V. All authors have given approval to the final version of the manuscript.

Competing interests

The authors declare no competing interests.